New Quaternary Compounds Resulting from the Reaction of Copper and f-Block Metals in Molten Polychalcogenide Salts at Intermediate Temperatures. Valence Fluctuations in the Layered $CsCuCeS_3$

Anthony C. Sutorik,[†] Joyce Albritton-Thomas,[‡] Tim Hogan,[‡] Carl R. Kannewurf,[‡] and Mercouri G. Kanatzidis*,[†]

Department of Chemistry, Michigan State University, East Lansing, Michigan 48824, and Department of Electrical Engineering and Computer Science, Northwestern University, Evanston, Illinois 60208

Received September 19, 1995. Revised Manuscript Received January 10, 1996[⊗]

From the reaction of elemental copper and either lanthanides or actinides in molten alkali metal/polychalcogenide salts, several new quaternary phases have been discovered. Specifically, these phases are $ACuM_2Q_6$ (where A = K, M = La, Q = S; A = Cs, M = Ce, Q = S; or A = K, M = Ce, Q = Se) and $ACuMQ_3$ (where A = Cs, M = Ce, Q = S; or A = K, M = U, Q = Se). The $CsCuCe_2S_6$ crystallizes in the orthorhombic space group *Immm* with a = 5.500(1) Å, b = 22.45(1) Å, c = 4.205(4) Å. The $KCuCe_2Se_6$ is isostructural. The $CsCuCeS_3$ crystallizes in the orthorhombic space group *Cmcm* with a = 4.024(2) Å, b = 15.154(2) Å, c = 10.353(3) Å. The $KCuUSe_3$ is isostructural. In $ACuM_2Q_6$, the lanthanides bond to a mixture of mono- and disulfides in a bicapped trigonal prismatic geometry; these polyhedra subsequently connect in two dimensions, forming layers equivalent to those seen in the $ZrSe_3$ structure type with Cu^+ atoms residing in tetrahedral sites within the layers and alkali cations in the interlayer gallery. The compounds of the formula $ACuMQ_3$ also possess a layered structure. Here the $[MQ_6]$ octahedral units form corrugated, two-dimensional sheets via edge-sharing in the first dimension and corner-sharing in the second. Copper cations are coordinated to tetrahedral sites in the folds of the corrugations, and alkali cations are again in the intergallery region. Details of the synthesis, structure, and properties of these compounds are discussed.

A. Introduction

The reactions of lanthanides in A_2Q_x fluxes have led to new phases which repeat several structural themes seen in known binary and ternary chalcogenides.[1] The next question to be asked is how can the reaction of these metals be modified in order to access phases which are less structurally related to known compounds and so more likely to feature new and novel characteristics. The simplest approach is to react another element, such as a transition metal, in the A_2Q_x flux along with the lanthanide or actinide with an eye toward forming new quaternary compounds. The extra element would be chosen such that its coordination chemistry is very different from that of the f-block metal. Thus, when the two metals come together in a new compound, the interplay of dissimilar structural and coordination requirements should help to maximize the probability that any new phases would be clear departures from what has been seen before. Investigations into quaternary systems with lanthanides and actinides are of particular interest because of the intriguing structural and physical properties which have been known to result from the interplay of covalent transition-metal bonding and the more ionic lanthanide and actinide bonding. For example, the most notable high-T_c copper oxide superconductors are compounds containing heterometallic mixtures of highly electropositive cations (i.e., $Tl_2Ba_2Ca_2Cu_3O_{10}$[2a] and $La_{2-x}(Ca, Sr, Ba)_xCuO_4$[2b,c]). It has been speculated that these cations have an inductive effect on the anionic Cu−O framework resulting in subtle changes in the covalency of those bonds which in turn impacts the critical temperature.[2,3] In the complicated cooperative environment of a solid-state material, there are many effects in which the cations may participate. A better understanding of the interplay of these effects could be achieved if a wider base of compounds containing mixtures of highly electropositive cations were available for study. As such we have been interested in searching for such compounds in quaternary systems containing the chalcogenide elements.

Many examples already exist of quaternary compounds isolated from reactions in molten A_2Q_x fluxes. Some systems have even been refined to the point where certain species can be formed reproducibly in situ and then used as ligands to the remaining metal cations in

[†] Michigan State University.
[‡] Northwestern University.
[⊗] Abstract published in *Advance ACS Abstracts,* February 15, 1996.

(1) (a) Sutorik, A. C.; Kanatzidis, M. G. *J. Am. Chem. Soc.* **1991**, *113*, 7754−7755. (b) Sutorik, A. C.; Kanatzidis, M. G. *Angew. Chem., Int. Ed. Engl.* **1992**, *31*, 1594−1596. (c) Sutorik, A. C. Kanatzidis, M. G., submitted for publication.

(2) (a) Sleight, A. W. *Chemistry of High-Temperature Superconductors*; ACS Symposium Series 351; American Chemical Society: Washington DC, 1987; Chapter 1, p 2. (b) Sheng, Z. Z.; Herman, A. M. *Nature* **1988**, *332*, 138−139. (c) Parkin, S. S.; et. al. *Phys. Rev. Lett.* **1988**, *61*, 750−753.

(3) (a) Bednorz, J. G.; Muller, K. A. *Z. Phys.* **1986**, *B64*, 189−193. (b) Cava, R. J.; vanDover, R. B.; Batlogg, B.; Reitman, E. A. *Phys. Rev. Letts.* **1987**, *58*, 408−410.

0897-4756/96/2808-0751$12.00/0

the flux. This approach has worked well in several quaternary systems where the fourth element is a nonmetal. The anion $(TeS_3)^{2-}$, which was employed as a ligand for the first time from a molten salt reaction,[4] and several thiophosphate and selenophosphate species have been isolated from the reaction of a metal and P_2Q_5 in excess A_2Q_x flux.[7−9] Mixed-metal reactions with Sn as one of the components have led to the characterization of phases in which either $(SnS_4)^{4-}$ or $(Sn_2S_6)^{4-}$ act as thiometalate ligands to the second metal.[10] A substantial body of work also exists where quaternary phases have been isolated from molten A_2Q_x the bulk of which has involved mixed metal reactions between Cu and early-transition-metal elements.[11−16] Recently, this work has been expanded into transition metal/f-block chemistry as well with the reporting of the compounds $BaLnMQ_3$ (Ln = La, Ce, Nd; M = Cu, Ag; Q = S, Se),[17] $KLnMQ_4$ (Ln = La, Nd, Ga, Y; M = Si, Ge; and Q = S, Se),[18] $CsCuUTe_3$,[19a] and $CsTiUTe_5$.[19b]

In attempting to develop similar quaternary chemistry with the f-block elements at intermediate temperatures (250−450 °C), several heterometallic systems were investigated. Of these systems the reactions using Cu were highly successful at providing new quaternary phases. Two new structure types have already been reported: $KCuCe_2S_6$ and $K_2Cu_2CeS_4$.[20] This report details the synthesis, structures, and properties of five new quaternary chalcogenides. Three of them are additions to the $KCuCe_2S_6$ family ($KCuLa_2S_6$, $CsCuCe_2S_6$, $KCuCe_2Se_6$) and two more phases ($CsCuCeS_3$ and $KCuUSe_3$) are isostructural to the known $ACuMQ_3$ structure type (A = alkali metal, M = 4^+ transition metal, Q = chalcogenide).[15,16]

B. Experimental Section

1. Synthesis. *Reagents.* The following reagents were used as obtained: copper metal, Fisher Scientific Co., Fairlawn, NJ; cerium, 40 mesh, Johnson M. Matthey Co., Ward Hill, MA; uranium metal, 60 mesh, Cerac, Milwaukee, WI; lanthanum, 40 mesh, Cerac, Milwaukee, WI; selenium powder, 100 mesh, Aldrich, Milwaukee, WI; sulfur powder, sublimed, JT Baker Co., Phillipsburg, NJ; potassium metal, analytical reagent, Mallinckrodt Inc., Paris, KY; sodium metal, analytical reagent, Mallinckrodt Inc., Paris, KY; cesium metal, Johnson M. Matthey Co., Ward Hill, MA; dimethylformamide (DMF), analytical reagent grade, EM Science, Inc., Gibbstown, NJ; methanol, anhydrous, analytical reagent grade, Mallinckrodt Inc., Paris, KY.

Potassium Selenide, K_2Se. The following procedure was modified from that given in the literature.[21] An amount of 4.976 g (127.3 mmol) K was sliced in an N_2-filled glovebox and combined with 5.024 g (63.6 mmol) of Se into a 250 mL round-bottom flask. The flask was chilled to −78 °C using a dry ice/acetone bath and approximately 100 mL of NH_3 was condensed, under an N_2 atmosphere, onto the reagents, giving a dark blue solution. The solution was stirred with a magnetic stir bar while the liquid NH_3 was allowed to slowly evaporate off as the reaction warmed to room temperature under a flow of N_2 (approximately 8 h). A second portion of NH_3 is usually added, and the evaporation repeated to ensure complete reaction of the reagents. The resulting light orange product is evacuated on a Schlenk line overnight and then taken into an N_2-filled glove box where it is ground to a fine powder and stored. Potassium sulfide (a pale yellow powder) was prepared and handled similarly.

Cesium Sulfide, Cs_2S. In an N_2-filled glovebox, 10.089 g (75.9 mmol) of Cs (**caution:** fire and explosion hazard if in contact with air or protic solvents!) is weighed into a 250 mL three-neck round-bottom flask. Two of the necks are stoppered, and the remaining one is connected to a glass adapter with a stopcock joint. The apparatus is removed from the box and connected to a coldfinger condenser adapted to allow for N_2 flow. The flask is chilled to −78 °C using a dry ice/acetone bath, and approximately 100 mL of NH_3 is condensed, under an N_2 atmosphere, onto the Cs, giving a dark blue solution. One of the flask stoppers is gently removed and, with N_2 flow maintained, a magnetic stir bar is added to the solution, followed by 1.217 g (38.0 mmol) of S once the solution is stirring. The remainder of the reaction proceeds as described above, resulting in a pale yellow product which was ground to a fine powder and stored in an N_2-filled glovebox.

$KCuLa_2S_6$. Amounts of 0.110 g (1.0 mmol) of K_2S, 0.016 g (0.25 mmol) of Cu, 0.069 g (0.50 mmol) of Ce, and 0.128 g (4.0 mmol) of S were weighed into a vial in an N_2-filled glovebox. The starting materials were mixed thoroughly and loaded into a Pyrex tube. The tube was then evacuated to $<3 \times 10^{-3}$ mbar and flame-sealed. In a computer-controlled furnace, the reaction was heated to 270 °C over 12 h, held at that temperature for 6 days, and cooled to 120 °C at 3 °C/h followed by quenching to 50 °C. The product was isolated by dissolving away residual K_2S_x flux with successive washing of degassed DMF under N_2 flow, in order to prevent oxidation of polysulfide to sulfur. Polysulfides dissolved in DMF are a dark blue-green solution when concentrated, and the isolation was continued by carefully decanting the concentrated DMF and replacing it with a fresh portion until such an addition remained clear, signaling complete K_2S_x removal. After isolation, a yellow powder remained which was confirmed as isostructural to $KCuCe_2S_6$[20] by comparison of the powder X-ray diffraction pattern of the product to that of the structurally known analogue. A yield of 89%, based on La, is typical. The product is insoluble in water, methanol, and DMF and appears stable in air for extended periods.

$CsCuCe_2S_6$. Amounts of 0.149 g (0.50 mmol) of Cs_2S, 0.016 g (0.25 mmol) of Cu, 0.070 g (0.50 mmol) of Ce, and 0.080 g (2.5 mmol) of S were weighed into a vial in an N_2-filled glovebox. The reagents were loaded into a Pyrex tube, and the tube was then evacuated to $<3 \times 10^{-3}$ mbar and flame-sealed. The reaction was heated to 400 °C over 12 h, held at that temperature for 3 days, and cooled to 200 °C at 4 °C/h followed by quenching to 50 °C. After removal of the excess flux (in the manner described above), a red/brown microcrystalline powder remained. The identity and purity of the material was confirmed by comparing the X-ray powder diffraction pattern of the product with one calculated using

(4) McCarthy, T.; Zhang, X.; Kanatzidis, M. G. *Inorg. Chem.* **1993**, *32*, 2944−2948.
(5) Zhang, X.; Kanatzidis, M. G. *J. Am. Chem. Soc.* **1994**, *116*, 1890−1898.
(6) Zhang, X.; Kanatzidis, M. G. *Inorg. Chem.* **1994**, *33*, 1238−1240.
(7) McCarthy, T. M.; Kanatzidis, M. G. *Chem. Mater.* **1993**, *5*, 1061−1063.
(8) McCarthy, T. M. Ph.D., Michigan State University, 1994.
(9) (a) McCarthy, T. M.; Kanatzidis, M. G. *J. Chem. Soc., Chem. Commun.* **1994**, 1089−1090. (b) McCarthy, T. M.; Kanatzidis, M. G. *Inorg. Chem.* **1995**, *34*, 1257−1267.
(10) Liao, J.-H.; Kanatzidis, M. G. *Chem. Mater.* **1993**, *5*, 1561−1569.
(11) Lu, Y.-J.; Ibers, J. A. *Inorg Chem.* **1991**, *30*, 3317−3320.
(12) Lu, Y.-J.; Ibers, J. A. *J. Solid State Chem.* **1991**, *94*, 381−385.
(13) Lu, Y.-J.; Ibers, J. A. *J. Solid State Chem.* **1993**, *107*, 58−62.
(14) Lu, Y.-J.; Ibers, J. A. *J. Solid State Chem.* **1992**, *98*, 312−317.
(15) Mansuetto, M. F.; Keane, P. M.; Ibers, J. A. *J. Solid State Chem.* **1992**, *101*, 257−264.
(16) Mansuetto, M. F.; Keane, P. M.; Ibers, J. A. *J. Solid State Chem.* **1993**, *105*, 580−587.
(17) (a) Christuk, A. E.; Wu, P.; Ibers, J. A. *J. Solid State Chem.* **1994**, *110*, 330−336. (b) Wu, P.; Christuk, A. E.; Ibers, J. A. *J. Solid State Chem.* **1994**, *110*, 337−344.
(18) Wu, P.; Ibers, J. A. *J. Solid State Chem.* **1993**, *107*, 347−355.
(19) (a) Cody, J. A.; Ibers, J. A. *Inorg. Chem.* **1995**, *34*, 3165−3172. (b) Cody, J. A.; Mansuetto, M. F.; Chien, S.; Ibers, J. A. *Mater. Sci. Forum* **1994**, *152−153*, 35−42.
(20) Sutorik, A. C.; Kanatzidis, M. G. *J. Am. Chem. Soc.* **1994**, *116*, 7706−7713.
(21) Feher, F. *Handbuch der Praparativen Anorganischen Chemie*; Brauer, G., Ed.; Fedinand Enke: Stuttgart, Germany, 1954; pp 280−281.
(22) McCarthy, T. J.; Tanzer, T. A.; Kanatzidis, M. G. *J. Am. Chem. Soc.* **1995**, *117*, 1294−1301.

data from the single-crystal study (see Supporting Information). The average yield was 80% based on Ce. The product is insoluble in water, methanol, and DMF and is stable in air for extended periods.

Single crystals of a size and quality sufficient for X-ray diffraction studies were grown from a reaction of 0.335 g (1.12 mmol) of Cs_2S, 0.008 g (0.125 mmol) of Cu, 0.035 g (0.25 mmol Ce) and 0.128 g (4.0 mmol) of S. The reagents were loaded into tubes as above and heated at 450 °C for 2 days followed by cooling to 200 °C at 4 °C/ h and quenching to 50 °C. After isolation with degassed DMF, a handful of large red needles of $CsCuCe_2S_6$ were manually removed from the bulk of the yellow powdery product, which was CeS_2 by powder X-ray diffraction.

$KCuCe_2Se_6$. Amounts of 0.157 g (1.0 mmol) of K_2Se, 0.032 g (0.50 mmol) of Cu, 0.070 g (0.50 mmol) of Ce, and 0.316 g (4.0 mmol) of Se were weighed into a vial in an N_2-filled glovebox. The reagents were loaded into a Pyrex tube, and the tube was then evacuated to $<3 \times 10^{-3}$ mbar and flame-sealed. The reaction was heated to 400 °C over 12 h, held at that temperature for 2 days, and cooled to 200 °C at 4 °C/h followed by quenching to 50 °C. After removal of the excess flux (in the manner described above), a black microcrystalline powder remained. The identity and purity of the material were confirmed by comparing the X-ray powder diffraction pattern of the product with one calculated using data from the single-crystal study (see Supporting Information). Typical yields were 40%, based on Ce. The product is insoluble in water, methanol, and DMF and is stable in air for extended periods. It is also a microcrystalline powder and so unsuitable of single-crystal X-ray diffraction studies. To grow crystals of the needed size, a reaction was run using half the amounts of the described reagents and with 2 days of heating at 450 °C (cooling at 4 °C/h to 250 °C followed by quenching to 50 °C). Although these modifications produced black, plank-shaped crystals of $KCuCe_2Se_6$ large enough for single-crystal study, the bulk product was not pure, being contaminated by some unknown species as evidenced by powder X-ray diffraction.

$CsCuCeS_3$. A single phase of $CsCuCeS_3$ was obtained by the reaction of 0.148 g (0.50 mmol) of Cs_2S, 0.016 g (0.25 mmol) of Cu, 0.035 g (0.25 mmol) of Ce, and 0.040 g (1.25 mmol) of S. The reagents were loaded into Pyrex tubes and evacuated to $<3 \times 10^{-3}$ mbar and flame-sealed. The reaction was heated to 400 °C over 12 h, held at that temperature for 4 days, and cooled to 200 °C in 50 h and to 50 °C in 1 h. The excess flux was removed by washing with one portion of degassed distilled water (left in contact with the sample for <15 min) and several portions of degassed DMF in the manner described previously. The remaining material was black microneedles. Purity is confirmed by comparing the X-ray powder diffraction pattern of the product to one calculated from single-crystal X-ray data (see Supporting Information). A small amount of CeO_2 (1−5%) is seen as an impurity. The yield was approximately 70%, based on Cu. The product is insoluble in methanol and DMF and appears stable in dry air for extended periods. Although stable in distilled water for a short time (<12 h), prolonged exposure is likely to decompose the phase due to the high oxophilicity of Ce^{3+}.

As is common in this chemistry, large single crystals suitable for X-ray diffraction studies were prepared via a separate method. In the case of $CsCuCeS_3$, a large amount of luck came into play, as the reaction has yet to be repeated. A mixture of 0.298 g (1.0 mmol) of Cs_2S, 0.008 g (0.126 mmol) of Cu, 0.018 g (0.128 mmol) of Ce, and 0.064 g (2.0 mmol) of S was prepared as previously. The reaction was heated at 390 °C for 5 days and cooled to 110 °C over 20 h, followed by further cooling to 50 °C over 1 h. Removal of the flux with three portions of degassed distilled water resulted in a very inhomogeneous product of which some large, black, plank-shaped crystals were one of the major components. These were the crystals subsequently used in the single-crystal X-ray determination of $CsCuCeS_3$. Sometimes while sealing the reactants in their Pyrex tube, an exothermic reaction occurs which splatters various amounts of the contents throughout the length of the tube. The origin of the exothermic reaction probably lies in there being a very small amount of unreacted Cs metal somewhere in the Cs_2S starting material.

$KCuUSe_3$. A single phase of $KCuUSe_3$ was obtained by the reaction of 0.078 g (0.50 mmol) of K_2Se, 0.032 g (0.50 mmol) of Cu, 0.120 g (0.50 mmol) of U, and 0.237 g (3.0 mmol) of Se. The reagents were loaded into Pyrex tubes and evacuated to $<3 \times 10^{-3}$ mbar and flame-sealed. The reaction was heated to 400 °C over 12 h, held at that temperature for 2 days, and cooled to 200 °C in 50 h and to 50 °C in 1 h. The excess flux was removed by washing with several portions of degassed DMF in the manner described previously. The remaining material was black needles. Purity was confirmed by comparing the X-ray powder diffraction pattern of the product to one calculated from single-crystal X-ray data (see Supporting Information), and typically, a small amount of USeO (<3%) is seen as an impurity. The yield of $KCuUSe_3$ is still nearly quantitative (90−95%). The product is insoluble in water, methanol, and DMF and appears stable in air for extended periods. Presumably, however, the compound is likely to decompose upon prolonged exposure to both air and water due to the highly oxophilic nature of the U^{4+}.

$KCuUSe_3$ is a particularly stable phase. Whereas the other compounds described in this paper have limited windows of temperature and flux composition for their formation, $KCuUSe_3$ is isolated from reactions run from 300 to 450 °C and with a metal to selenium ratio as high as $^1/_{24}$. All of these other conditions produce varying amounts of elemental Se as a major contaminant, but no evidence of phase separation of the metal reactants into binary or ternary compounds was observed.

2. Physical Measurements. *Powder X-ray Diffraction.* Analyses were performed using a calibrated Rigaku Rotaflex rotating anode powder diffractometer controlled by an IBM computer and operating at 45 kV/100 mA, employing Ni-filtered Cu radiation. Samples are ground to a fine powder and mounted by spreading the sample onto a piece of double-sided Scotch tape affixed to a glass slide. For air-sensitive compounds, samples were prepared in an N_2-filled glovebox and coated with mineral oil before analysis. Powder patterns were calculated by using the CERIUS molecular modeling program by Molecular Simulations, St. John's Innovation Centre, Cambridge, England.

Infrared Spectroscopy. Infrared spectra, in the far-IR region (600−50 cm^{-1}), were recorded on a computer-controlled Nicolet-740 Fourier transform infrared spectrophotometer in 4 cm^{-1} resolution. Analyses were performed on finely ground solid samples using CsI as the pressed pellet matrix. For air-sensitive compounds, samples were prepared in an N_2-filled glovebox and pressed into a pellet immediately upon removal.

Solid State UV/Vis/Near-IR Spectroscopy. Optical diffuse reflectance measurements were performed at room temperature using a Shimadzu UV-3101PC double-beam, double-monochromator spectrophotometer. The instrument is equipped with integrating sphere and controlled by personal computer. The data were processed as reported earlier.

Magnetic Susceptibility. The magnetic response of the compounds was measured over the range 2−300 K using a MPMS Quantum Design SQUID magnetometer. Samples were ground to a fine powder to minimize possible anisotropic effects and loaded into PVC containers. Air-sensitive samples were prepared in a drybox. Corrections for the diamagnetism of the sample containers were made by measuring the magnetic response of the empty container under the same conditions of temperature and field which were measured for the filled container. Core atom diamagnetism was much smaller than the magnitude of the paramagnetism measured and so was ignored. Magnetic susceptibility as a function of field strength (at a constant temperature of 300 K) was first investigated to determine if the samples experienced saturation of their magnetic signal. For all compounds, magnetization increased linearly with increasing field over the range investigated (100−55 000 G). The subsequent temperature dependent studies were performed at low-to-moderate field strengths (300−5000 G).

Charge-Transport Measurements. Dc electrical conductivity studies and thermopower measurements were performed either on single crystals or pressed polycrystalline pellets depending on the availability of each sample. Conductivity measurements were performed in the usual four-probe geom-

Table 1. Crystallographic Data for $CsCuCe_2S_6$, $KCuCe_2Se_6$, $CsCuCeS_3$, and $KCuUSe_3$

	$CsCuCe_2S_6$	$KCuCe_2Se_6$
a, Å	5.500(1)	5.695(1)
b, Å	22.45(1)	22.236(6)
c, Å	4.205(4)	4.297(2)
β, deg	90	90
V, Å^3	519.3(6)	544.1(3)
space group	*Immm* (No. 71)	*Immm* (No. 71)
Z	2	2
FW, g/mol	669.05	856.64
d_{calc}, g/cm^3	4.279	5.228
μ, cm^{-1}	153.28	305.05
crystal dimensions, mm^3	0.01 × 0.04 × 0.24	0.02 × 0.06 × 0.44
radiation	Mo, Kα	Mo, Kα
2θ max, deg	60.0	60.0
data collection temp, °C	23	−100
no. data collected	451	494
no. unique data	451	494
no. $F_o^2 > 3\sigma(F_o^2)$	384	396
no. of variables	22	22
R/R_w,[a] %	3.4/4.3	3.5/4.2
final dif map max peak, e$^-$/Å^3	1.54	1.42
	$CsCuCeS_3$	$KCuUSe_3$
a, Å	4.024(2)	4.112(2)
b, Å	15.154(2)	14.437(3)
c, Å	10.353(3)	10.675(2)
β, deg	90	90
V, Å^3	631.3(4)	633.7(3)
space group	*Cmcm* (No. 63)	*Cmcm* (No. 63)
Z	4	4
FW, g/mol	423.75	577.55
d_{calc}, g/cm^3	4.552	6.719
μ, cm^{-1}	170.84	243.2
crystal dimensions, mm^3	0.02 × 0.10 × 0.22	0.02 × 0.04 × 0.20
radiation	Mo, Kα	Mo, Kα
2θ max, deg	59.9	60.0
data collection temp, °C	−100	23
no. of data collected	532	536
no. of unique data	532	517
no. of $F_o^2 > 3\sigma(F_o^2)$	450	401
no. of variables	23	23
R/R_w,[a] %	3.2/4.2	3.3/4.2
final dif map max peak, e$^-$/Å^3	1.70	2.61

[a] $R = \sum(|F_o| - |F_c|)/\sum|F_o|$. $R_w = \{\sum_w(|F_o| - |F_c|)^2/\sum w|F_o|^2\}^{1/2}$.

etry with 60- and 25-μm diameter gold wires used for the current and voltage electrodes, respectively. Measurements of the sample cross-sectional area and voltage probe separation were made with a calibrated binocular microscope. Conductivity data were obtained with the computer-automated system described elsewhere.[23] Thermoelectric power measurements were made by using a slow ac technique[24] which requires the production of a slowly varying periodic temperature gradient across the samples and measuring the resulting sample voltage. Samples were suspended between quartz block heaters by 60-μm gold wires thermally grounded to the block with GE 7031 varnish. The gold wires were used to support and conduct heat to the sample, as well as to measure the voltage across the sample resulting from the applied temperature gradient. The magnitude of the applied temperature gradient was generally 1.0 K. Smaller temperature gradients gave essentially the same results but with somewhat lower sensitivity. In both measurements, the gold electrodes were held in place on the sample with conductive gold paste. Mounted samples were placed under vacuum (10^{-3} Torr) and heated to 320 K for 2−4 h to cure the gold contacts. For a variable-temperature run, data (conductivity or thermopower) were acquired during sample warming. The average temperature drift rate during an experiment was kept below 0.3 K/min.

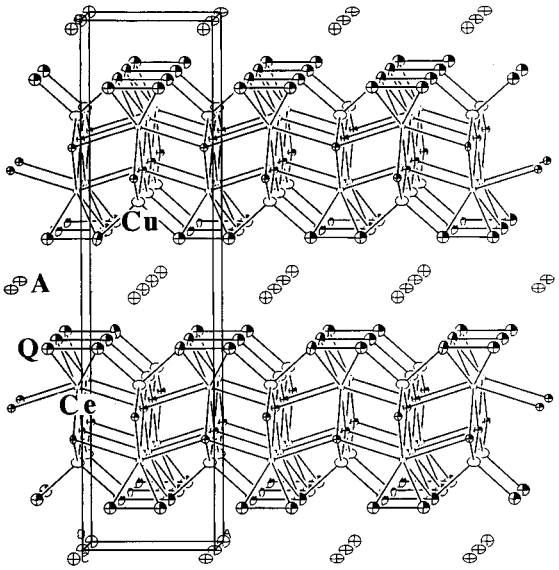

Figure 1. Extended structure of the orthorhombic form of $ACuCe_2Q_6$ as seen down the *a* axis (circles with nonshaded octants, A; large open circles, Cu; small open circles, Ce; circles with shaded octants, Q).

Multiple variable-temperature runs were carried out for each sample to ensure reproducibility and stability. At a given temperature, reproducibility was within ±5%.

Single-Crystal X-ray Diffraction. Intensity data were collected using a Rigaku AFC6S four-circle automated diffractometer equipped with a graphite crystal monochromator. An $\omega-2\theta$ scan mode was used. Crystal stability was monitored with three standard reflections whose intensities were checked every 150 reflections, and unless noted, no crystal decay was detected in any of the compounds. An empirical absorption correction based on ψ scans was applied to all data during initial stages of refinement. An empirical DIFABS correction[25] was applied after full isotropic refinement, after which full anisotropic refinement was performed. The structures were solved by direct methods using SHELXS-86 software[26a] (for all compounds), and full-matrix least-squares refinement was performed using the TEXSAN software package.[26b] Crystallographic data for the compounds in this section are given in Table 1.

C. Results and Discussion

1. $ACuLn_2Q_6$. *Structure.* Phases with this stoichiometry have been found to crystallize in either the monoclinic space group *C*2/*c* for $KCuLn_2S_6$ (Ln = La, Ce)[20] or the orthorhombic space group *Immm* for $CsCuCe_2S_6$ and $KCuCe_2Se_6$; see Table 1. The lack of single-crystal studies on $KCuLa_2S_6$, of course, precludes any detailed discussion of its structural features; however, it is expected that slight contractions in bond angles would occur upon replacing the larger Ce^{3+} with the smaller La^{3+}. Although of a higher symmetry than $KCuCe_2S_6$, the orthorhombic $CsCuCe_2S_6$ and $KCuCe_2Se_6$ have essentially the same structure, the latter two compounds simply have a fewer number of symmetry-independent atoms relative to the monoclinic form.

A view of the structure of the orthorhombic compounds is given in Figure 1. The Ln atoms are coordinated by a bicapped trigonal prism of Q atoms made of two $(Q_2)^{2-}$ units forming the short sides of the prism

(23) Lyding, J. W.; Marcy, H. O.; Marks, T. J.; Kannewurf, C. R. *IEEE Trans. Instrum. Meas.* **1988**, *37*, 76−80.
(24) Marcy, H. O.; Marks, T. J.; Kannewurf, C. R. *IEEE Trans. Instrum. Meas.* **1990**, *39*, 756−760.
(25) Walker, N.; Stuart, D. *Acta Crystallogr.* **1983**, *A39*, 158−166.
(26) (a) Sheldrick, G. M. In *Crystallographic Computing 3*; Sheldrick, G. M., Kruger, C., Doddard, R., Eds.; Oxford University Press: Oxford, England, 1985; pp 175−189. (b) Gilmore G. J. *Appl. Cryst.* **1984**, *17*, 42−46.

Table 2. Fractional Atomic Coordinates and *B*(eq)[a] Values for $CsCuCe_2S_6$ with Estimated Standard Deviations in Parentheses

atom	*x*	*y*	*z*	*B*(eq)[a]
Ce	$-1/2$	0.18509(4)	0	0.77(3)
Cs	0	0	0	2.21(6)
Cu[b]	−1	0.1731(2)	$-1/2$	1.7(2)
S(1)	−1	0.2249(2)	0	0.9(2)
S(2)	−0.6898(5)	0.1043(2)	$-1/2$	2.1(2)

[a] *B* values for anisotropically refined atoms are given in the form of the isotropic equivalent displacement parameters defined as $B(eq) = 4/3[a^2B(1,1) + b^2B(2,2) + c^2B(3,3) + ab(\cos\gamma)B(1,2) + ac(\cos\beta)B(1,3) + bc(\cos\alpha)B(2,3)]$. [b] Occupancy is 0.5.

Table 3. Fractional Atomic Coordinates and *B*(eq)[a] Values for $KCuCe_2Se_6$ with Estimated Standard Deviations in Parentheses

atom	*x*	*y*	*z*	*B*(eq)[a]
Ce	$1/2$	0.17980(4)	0	0.49(3)
Cu[b]	0	0.1735(2)	$-1/2$	1.5(2)
K	0	0	−1	1.7(2)
Se(1)	0	0.22420(4)	0	0.57(6)
Se(2)	0.2916(2)	0.09526(7)	$-1/2$	1.40(5)

[a] *B* values for anisotropically refined atoms are given in the form of the isotropic equivalent displacement parameters defined as $B(eq) = 4/3[a^2B(1,1) + b^2B(2,2) + c^2B(3,3) + ab(\cos\gamma)B(1,2) + ac(\cos\beta)B(1,3) + bc(\cos\alpha)B(2,3)]$. [b] Occupancy is 0.5.

and four Q^{2-} ions at the apex and capping positions. Anionic layers are formed when the trigonal prisms stack in one dimension by sharing triangular faces and neighboring stacks cap each other by sharing monosulfide ions in the second dimension. The space between the chains of prisms contains Cu atoms residing in tetrahedral sites formed by two bonds to two monochalcogenides and two bonds to one atom on two separate dichalcogenides. Of particular note is that the Cu site occupancy disorder observed in $KCuCe_2S_6$ is repeated in the case of the orthorhombic analogues. In that first member of this family, two crystallographically distinct Cu^+ sites exist, one with an occupancy of 85% and the other, only 15%. The higher symmetry of the orthorhombic space group requires there be only one Cu site, but the occupancy of that site refines at 50%, meaning that, on the average, a Cu atom is present only half of the time. The alkali cations remain fully occupied in both crystallographic modifications. This implies that a full layer of alkali cations is needed for lattice stabilization regardless of the space group, and the phases seem to have the ability to pull in only enough Cu^+ ions to achieve neutrality.

The fractional atomic coordinates of the two orthorhombic phases are given in Tables 2 and 3. A fragment showing the immediate coordination environments of the metals is shown in Figure 2, and selected bond distances are given in Table 4. The Ce−S distances in $CsCuCe_2S_6$ range from 2.892(1) to 2.967(3) Å and are comparable with those found in compounds such as $KCeS_2$ (2.878 Å[27]), CeS_2 (2.88−3.26 Å[28]), while the disulfide bond is 2.088(6) Å. The distances for selenide analogue are in line with what would be expected for both the Ce−Se values (3.0136(9)−3.092(1) Å) and the diselenide distance (2.374(3) Å). For example in $KCeSe_4$ the Ce−Se distance is 3.075 Å and the Se−Se distance, 2.385 Å.[1b] In both compounds, the chalcogenide bonds about the Cu^+ are typical.

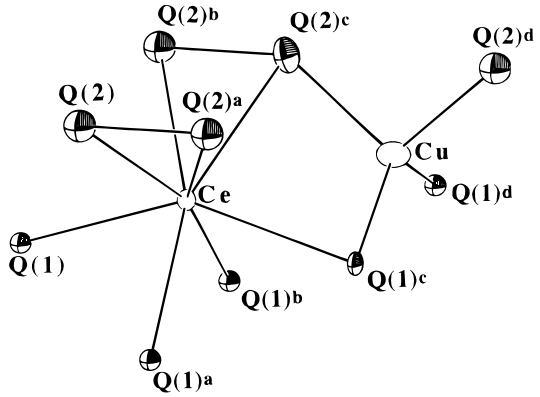

Figure 2. Fragment of the anionic structure of $ACuCe_2Q_6$ (A = Cs, Q = S; A = K, Q = Se) highlighting the coordination environment of the Cu and Ce atoms.

Table 4. Selected Bond Distances (Å) and Angles (deg) for $CsCuCe_2S_6$ and $KCuCe_2Se_6$ with Standard Deviations in Parentheses[a]

	$CsCuCe_2S_6$	$KCuCe_2Se_6$
Ce-Q(1)	2.892(1)	3.0136(9)
Ce-Q(1)[a,b]	2.917(3)	3.029(2)
Ce−Q(2)	2.967(3)	3.092(1)
Cu−Q(1)[c,d]	2.403(3)	2.426(3)
Cu−Q(2)[c,d]	2.302(4)	2.405(4)
Q(2)−Q(2)[a]	2.088(6)	2.374(3)
A−Q(2)	3.580(3)	3.444(1)
Q(1)−Ce−Q(1)[a]	77.64(4)	76.65(2)
Q(1)−Ce−Q(1)[b]	144.0(1)	141.76(7)
Q(1)[a]−Ce−Q(1)[c]	92.3(1)	90.36(6)
Q(1)−Ce−Q(2)	81.62(8)	80.59(4)
Q(1)−Ce−Q(2)[a]	121.57(7)	124.19(3)
Q(1)[a]−Ce−Q(2)	85.00(9)	86.31(4)
Q(1)[a]−Ce−Q(2)[b]	159.18(6)	157.15(3)
Ce−Q(2)[c]−Cu	81.4(1)	79.93(7)
Ce−Q(1)[c]−Cu	81.41(6)	81.25(4)
Q(1)[c]−Cu−Q(1)[d]	122.1(2)	124.6(2)
Q(1)[c]−Cu−Q(1)[a]	108.95(7)	109.64(5)
Q(1)[a]−Cu−Q(1)[d]	95.7(2)	87.3(2)

[a] The superscipted letters indicate the atom labeling in the corresponding figure.

The $ACuLn_2Q_6$ family turns out to have the same Ln/Q framework as that found in the ternary phases $NaLnS_3$.[1c] That framework is analogous to the $ZrSe_3$ structure type.[29] Figure 3 shows a side-by-side comparison of the structures of $NaLnS_3$ and $ACuLnQ_3$.

The interlayer grooves undergo some slight modifications between the ternary and quaternary structures, responding to the absence or presence of Cu^+ cations. Two parameters give a good idea about the general size of the groove: the Ce−S−Ce angle along the bottom of the groove and the S−S distance across the top. In $NaCeS_3$ these values are 155.2° and 3.58 Å, respectively, while in $KCuCe_2S_6$ they are 143.2° and 3.36 Å and in $CsCuCe_2S_6$, 144.0° and 3.41 Å. Apparently, without the covalent interactions of Cu atoms, the grooves are free to open up somewhat, implying that they may be able to accommodate cations over a limited range of sizes.

The disorder observed in the Cu atom positions of both $ACuM_2Q_6$ structure types, coupled with the fact that those sites are totally empty in $NaLnS_3$ phases, gives reasonable indication that these phases would

(27) (a) Plug, C. M.; Verschoor, G. C. *Acta Crystallogr.* **1976**, *B32*, 1856−1858. (b) Ohtani, T.; Honjo, H.; Wada, H. *Mater. Res. Bull.* **1987**, *22*, 829−840.

(28) (a) Marsh, R. E.; Herbstein, F. H. *Acta Crystallogr.* **1983**, *39B*, 280−287. (b) Yanagisawa, Y.; Kanamaru, F.; Kume, S. *Acta Crystallogr.* **1979**, *35B*, 137−139.

(29) Kroniert, W.; Plieth, K. *Z. Anorg. Allg. Chem.* **1965**, *336*, 207−218.

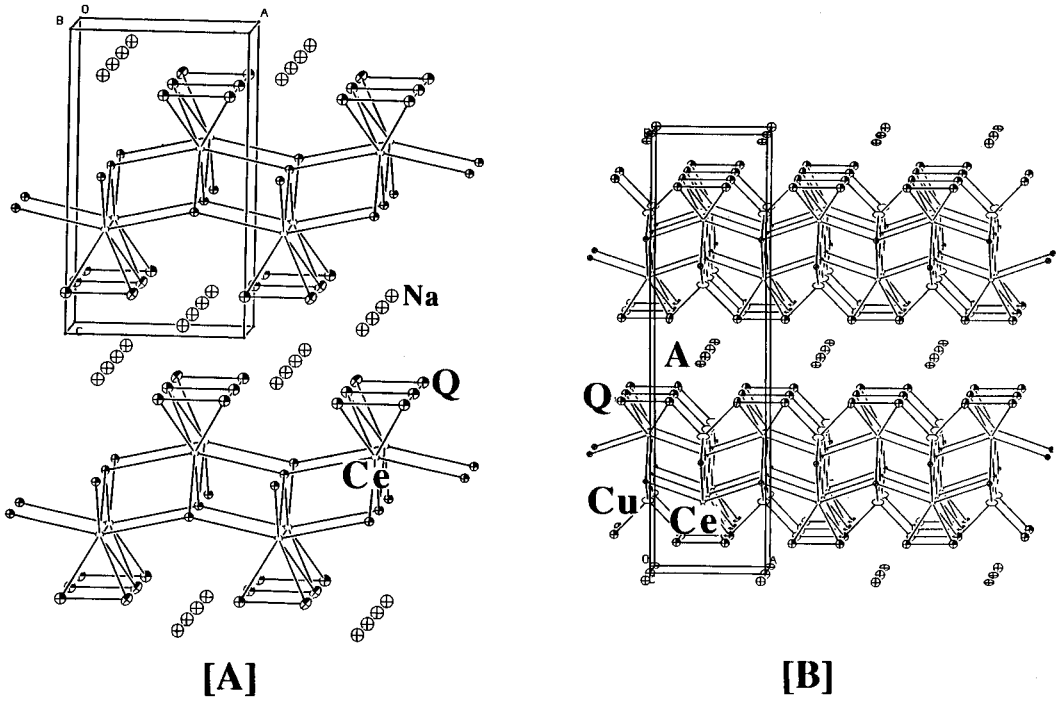

Figure 3. (A) Extended structure of the $NaLnS_3$ structure type. (B) Extended structure of the $ACuLn_2Q_6$ structure type (circles with nonshaded octants, A; large open circles, Cu; small open circles, Ce; circles with shaded octants, Q).

have appreciable Cu^+ mobility through the intralayer grooves. Such mobility would also allow for ion-exchange capabilities. Even reductive intercalation chemistry could be possible in these phases; the compound TiS_3, isostructural to $ZrSe_3$, is known to undergo Li^+ intercalation after the reduction of the $(Se-Se)^{2-}$ units to $2Se^{2-}$ with *n*-BuLi.[30]

From the discussion so far, one can reasonably postulate the existence of two structurally related compounds: $CuLnQ_3$ and $ALnQ_3$ (A = K, Cs). The former, with all Cu^+ sites at full occupancy, would have the interlayer galleries cleared of counterions creating a van der Waals gap. The $ALnQ_3$, with the extra alkali ions in a bilayer such as in $NaLnS_3$, would have totally empty intralayer grooves. There is no obvious reason why $CuLnQ_3$ should not exist, and it might be formed from fluxes of reduced alkali cation content.

Ternary molten A_2Q_x reactions in the Cs/Ce/S system invariably led to CeS_2 under S-rich conditions and to $CsCeS_2$ under basic, S-poor conditions. Similar results were observed in the potassium system, although one phase was obtained whose X-ray powder diffraction pattern bore similarities to the orthorhombic $ACuLn_2Q_6$ phases.[31] Elemental analysis revealed an average composition of $K_{1.5}Ce_{2.5}S_{6.5}$, but single crystals of this phase could not be grown.

Magnetic Susceptibility Studies. The temperature-dependent magnetic susceptibility of $CsCuCe_2S_6$, taken at 2000 G over the range 2−300 K, is shown in Figure 4. Curie−Weiss behavior is evident with some local antiferromagnetic ordering at low temperatures. Below 100 K, the data deviate negatively from a straight line extrapolated from higher temperatures. This phenomenon has been observed in other Ce^{3+} chalcogenides and has been attributed to crystal field splitting of the cation's $^2F_{5/2}$ ground state.[32] The data conform to a

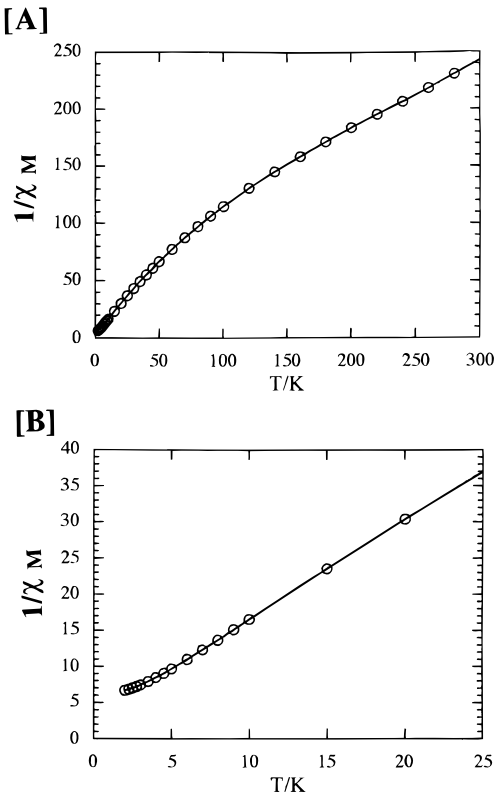

Figure 4. Inverse molar magnetic susceptibility ($1/\chi_M$) plotted against temperature (2−300 K) for $CsCuCe_2S_6$ (2000 G). (B) Expanded view of the region 2−25 K.

straight line at temperatures above 100 K and in that region a μ_{eff} of 3.1 μB for $CsCuCe_2S_6$ was calculated by applying a straight-line curve fit to the data. Since there are two Ce^{3+} ions (hence two $4f^1$ electrons) per formula, we estimate a μ_{eff} of 2.1 μB per Ce^{3+}. This is close to both the values seen experimentally (2.3−2.5

(30) Murphy, D. W.; Trumbore, F. A. *J. Electrochem. Soc.* **1976**, *123*, 960−964.
(31) Sutorik, A. C.; Kanatzidis, M. G., unpublished results.
(32) (a) Lueken, H.; Bruggemann, W.; Bronger, W.; Fleischhauer, V. *J. Less-Common Met.* **1979**, *65*, 79−88. (b) Duczmal, M.; Pawlak, L. *J. Magn. Magn. Mater.* **1988**, *76−77*, 195−196.

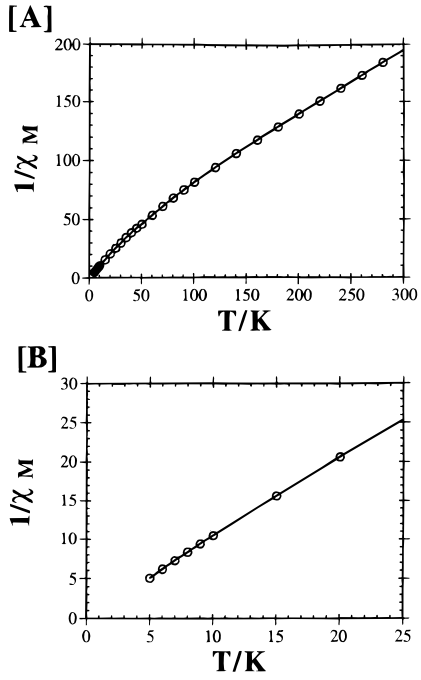

Figure 5. Inverse molar magnetic susceptibility ($1/\chi_M$) plotted against temperature (2−300 K) for $KCuCe_2Se_6$ (2000 G). (B) Expanded view of the region 2−25 K.

μB) and to the calculated theoretical value (2.54 μB) for a Ce^{3+} ion.[33] Lanthanides in general have μ_{eff} values which seldom vary with the chemical environment due to the shielding effect the valence orbitals have on the more "deeply buried" 4f electrons. A value of −96 K for the Weiss constant, θ, was also estimated from the high-temperature data, indicating a fairly substantial amount of local antiferromagnetic ordering.

The shielding of the $4f^1$ electrons causes the magnetic response of the Ce^{3+} cations in $KCuCe_2Se_6$ to strongly resemble to that observed in $CsCuCe_2S_6$. For the selenium analog (Figure 5) the high temperature μ_{eff} was estimated at 2.4 μB, but the θ changes to about −47 K, indicating that in this coordination geometry the Se 4p orbitals are somehow less conducive to superexchange-mediated, antiferromagnetic ordering between Ce^{3+} ions than the S 3p orbitals.

Magnetic studies were not performed on $KCuLa_2S_6$ because La^{3+} is a $4f^0$ cation and is expected to be diamagnetic.

Spectroscopic Data. The optical absorption spectra of the sulfide analogues of $ACuLn_2Q_6$ are shown in Figure 6, with the previously reported data for $KCuCe_2S_6$ included for comparison. From the steepest slope of the absorbance data we estimated the bandgap for $KCuCe_2S_6$ and $CsCuCe_2S_6$ to be 1.8 and 2.0 eV and for $KCuLa_2S_6$, 2.4 eV. Hence, these phases are expected to be semiconductors. This, in conjunction with the magnetic studies, confirms the valence precise nature of these materials, and so oxidation states can be formalized as $A(Cu^{1+})(Ln^{3+})_2(Q^{2-})_2(Q_2^{2-})_2$. The tail of absorbance occurring below the band edge for both $KCuCe_2S_6$ and $CsCuCe_2S_6$ may indicate either spectroscopic impurities or the presence of an indirect bandgap character to the electronic structure. The black $KCuCe_2Se_6$ shows only weak absorbance, but by extrapolating the absorption edge to zero, a bandgap of 0.55 eV can be estimated.

(33) Greenwood, N. N.; Earnshaw, A. *Chemistry of the Elements*; Pergamon Press: New York, 1984; p 1443.

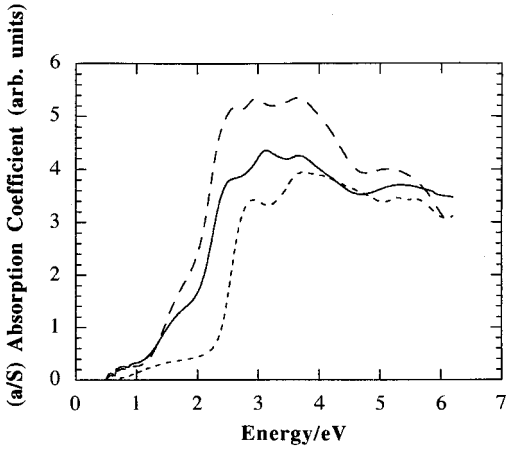

Figure 6. Solid-state diffuse reflectance spectra of $KCuCe_2S_6$ (—), $CsCuCe_2S_6$ (— — —), and $KCuLa_2S_6$ (- - -) plotted as absorption coefficient (α/S) vs energy (eV).

Table 5. Peaks from the Far-IR Spectra of $KCuCe_2S_6$, $KCuLa_2S_6$, $CsCuCe_2S_6$, and $KCuCe_2Se_6$

$KCuCe_2S_6$ (cm^{-1})	$KCuLa_2S_6$ (cm^{-1})	$CsCuCe_2S_6$ (cm^{-1})	$KCuCe_2Se_6$ (cm^{-1})
473 (m)	468 (m)	475 (m)	
358 (w)			
307 (w)			
264 (s)			
258 (s)	250 (s)	258 (s)	263 (m)
214 (s)	212 (s)	217 (s)	
204 (s)	198 (s)	202 (s)	200 (s)
156 (s)	150 (s)	175 (s)	172 (s)
		148 (s)	141 (s)
			131 (s)

Peaks from the far-IR spectra of all $ACuLn_2Q_6$ analogues are summarized in Table 5. For the sulfides, peaks in three general regions are observed. A medium-to-weak intensity peak occurs from 468 to 475 cm^{-1}, which corresponds to a S−S stretching vibration. From 302 to 358 cm^{-1} are very weak and broad peaks which are presumably due to Cu−S bonds, the disordered nature of which probably contributes to their small intensities. Finally, a series of very strong peaks occurs in the region from 270 to 148 cm^{-1} and have been assigned as mainly Ce−S vibrations.

In the far-IR spectrum of $KCuCe_2Se_6$ a medium-intensity peak of 264 cm^{-1} is observed which corresponds to a Se−Se vibration. As with the sulfides, a manifold of low-energy peaks (132−199 cm^{-1}) is assigned to Ce−Se vibrations. Presumably, vibrations for the Cu−Se bond would appear at slightly higher energies than that of the Se−Se bond, but in fact none are observed. These vibrations must be either too weak to be seen or are simply IR inactive.

2. The $ACuMQ_3$ (A = Cs, M = Ce, Q = S; or A = K, M = U, Q = Se) Family and Valence Fluctuations. *Structure.* In the structure of the $ACuMQ_3$ phases the f-block metal is coordinated to an octahedron of monochalcogenides. These $[MQ_6]$ units share edges with each other, forming one-dimensional chains parallel to the *a* axis. These chains of octahedra are further connected through corner-sharing into a corrugated two-dimensional sheet; see Figure 7. The overall anionic network remains layered as the Cu^+ cations occupy tetrahedral sites in the folds of the layers of octahedra and so provide no extra dimensionality to the framework; see Figure 8. The alkali cations reside within the interlayer galleries. If the Cu^+ were to be ignored, the remaining atoms would possess the anti-Pd_3Te_2 struc-

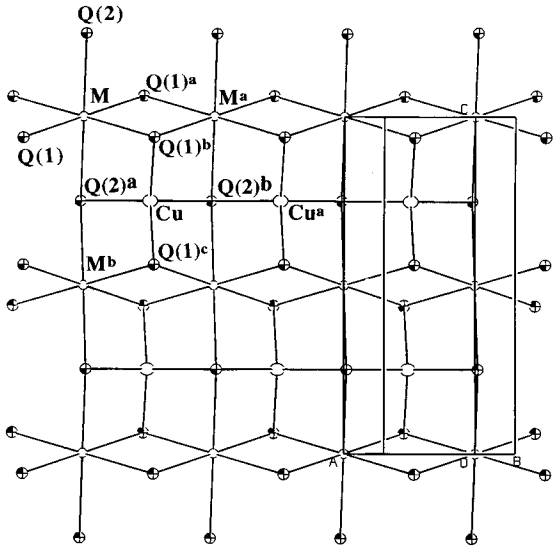

Figure 7. View perpendicular to a single anionic layer of the $ACuMQ_3$ structure type, where A = Cs, M = Ce, Q = S; or A = K, M = U, Q = Se (large open circles, Cu; small open circles, M, circles with shaded octants, Q).

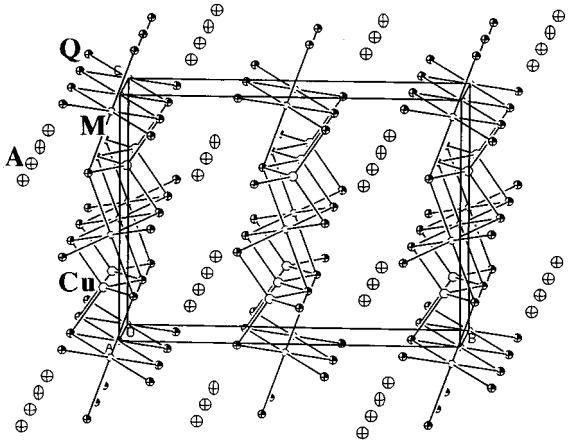

Figure 8. The $ACuMQ_3$ structure type (A = Cs, M = Ce, Q = S; or A = K, M = U, Q = Se) as seen down the a axis, parallel to the anionic layers (circles with nonshaded octants, A; large open circles, Cu; small open circles, M, circles with shaded octants, Q).

ture type in which Te atoms occupy both the octahedral sites and the interlayer gallery positions.[34] An example of a ternary compound with this structure is $BaIrO_3$.[35] Interestingly, $BaUS_3$ is a known phase as well[36] but possesses a distorted perovskite structure in which $[US_6]$ octahedra corner-share in three dimensions, instead of forming the two-dimensional layers of $ACuMQ_3$. This structure type has been seen in the recently reported Te analogue of the compound[19a] and in several several quaternary phases containing tetravalent early-transition-metal cations.[15,16]

The $ACuMQ_3$ phases also share some structural features with the previously reported phase $K_2Cu_2CeS_4$.[20] Both structures possess anionic layers built from $[CuQ_4]$ tetrahedra and $[MQ_6]$ octahedra, but in $K_2Cu_2CeS_4$ the connectivity of the octahedra is limited to one dimension, forming a series of edge-sharing infinite chains. These chains are subsequently joined into layers via intervening $[CuS_4]$ tetrahedra. Bond distances for $CsCuCeS_3$ are summarized in Table 7. While the Cu−S distances remain consistent with those that have been observed in other phases, the Ce−S distances are slightly shorter than is normal (2.712 and 2.730 Å vs 2.93 Å for an average 6-coordinate Ce^{3+} [37]). For $KCuUSe_3$ bond distances about both the U and Cu are as expected; see Table 6. The atomic coordinates for $CsCuCeS_3$ are given in Table 7 and for $KCuUSe_3$ in Table 8.

In another similarity to $K_2Cu_2CeS_4$, the formal oxidation states of the elements in $CsCuCeS_3$ do not balance with the known chemical limitations of Cu and Ce in their chalcogenide chemistry. A formalism with all S^{2-} would require either a Cu^{2+} or Ce^{4+} to achieve charge neutrality, and since both are very oxidizing relative to S^{2-}, there is the likelihood of a S^- state being present but delocalized through the sulfur 3p band. This is

Table 6. Selected Bond Distances (Å) and Angles (deg) for $CsCuCeS_3$ and $KCuUSe_3$ with Standard Deviations in Parentheses

	$CsCuCeS_3$	$KCuUSe_3$
M−Q(1)	2.730(2)	2.848(1)
M−Q(2)	2.712(1)	2.839(1)
Cu−Q(1)	2.319(3)	2.447(3)
Cu−Q(2)	2.413(2)	2.514(3)
A−Q(2)	3.474(3)	3.299(5)
Q(1)−M−Q(1)^a	180.00	180.00
Q(1)−M−Q(1)^b	94.93(9)	92.41(5)
Q(1)^a−M−Q(1)^b	85.07(9)	87.59(5)
Q(1)^a−M−Q(2)	91.41(7)	90.47(5)
Q(1)^b−M−Q(2)	88.59(7)	89.53(5)
Q(2)−M−Q(2)^a	180.00	180.00
Q(1)^b−Cu−Q(1)^c	116.7(1)	111.1(2)
Q(1)^b−Cu−Q(2)^a	106.84(5)	108.99(3)
Q(2)^a−Cu−Q(2)^b	113.0(2)	109.7(2)
M−Q(1)−M^a	94.93(9)	92.41(5)
M−Q(1)^b−Cu	81.77(7)	79.58(6)
M−Q(2)−M^b	145.3(1)	140.1(1)
M−Q(2)^a−Cu	80.53(6)	78.67(4)
Cu−Q(2)^b−Cu^a	113.0(2)	109.7(2)

Table 7. Fractional Atomic Coordinates and *B*(eq)^a Values for $CsCuCeS_3$ with Estimated Standard Deviations in Parentheses

atom	*x*	*y*	*z*	*B*(eq)^a
Ce	0	0	$^1/_2$	0.42(3)
Cu	0	0.5345(1)	$^1/_4$	0.74(6)
Cs	0	0.25980(6)	$^1/_4$	0.92(3)
S(1)	0	−0.0533(2)	$^1/_4$	0.5(1)
S(2)	0	0.3851(2)	0.5593(2)	0.66(8)

^{a} *B* values for anisotropically refined atoms are given in the form of the isotropic equivalent displacement parameters defined as $B(\text{eq}) = (^4/_3)[a^2B(1,1) + b^2B(2,2) + c^2B(3,3) + ab(\cos\gamma)B(1,2) + ac(\cos\beta)B(1,3) + bc(\cos\alpha)B(2,3)]$.

Table 8. Fractional Atomic Coordinates and *B*(eq)^a Values for $KCuUSe_3$ with Estimated Standard Deviations in Parenthese

atom	*x*	*y*	*z*	*B*(eq)^a
U	0	0	$^1/_2$	0.74(3)
Cu	$-^1/_2$	−0.0331(2)	$^1/_4$	1.4(1)
K	$-^1/_2$	−0.2458(4)	$^3/_4$	2.0(2)
Se(1)	$-^1/_2$	−0.1289(1)	0.4390(1)	1.02(6)
Se(2)	0	0.0671(2)	$^1/_4$	0.95(8)

^{a} *B* values for anisotropically refined atoms are given in the form of the isotropic equivalent displacement parameters defined as $B(\text{eq}) = (^4/_3)[a^2B(1,1) + b^2B(2,2) + c^2B(3,3) + ab(\cos\gamma)B(1,2) + ac(\cos\beta)B(1,3) + bc(\cos\alpha)B(2,3)]$.

(34) Matkovic, P.; Schubert, K. *J. Less-Common Met.* **1977**, *52*, 217−220.
(35) Rodi, V. F.; Babel, D. *Z. Anorg. Allg. Chem.* **1965**, *336*, 17−23.
(36) Lelieveld, R.; Ijdo, D. J. W. *Acta Crystallogr.* **1980**, *36B*, 2223−2226.
(37) Poix, P. *C. R. Acad. Sci. Paris, Ser. C* **1970**, *270*, 1852−1853.

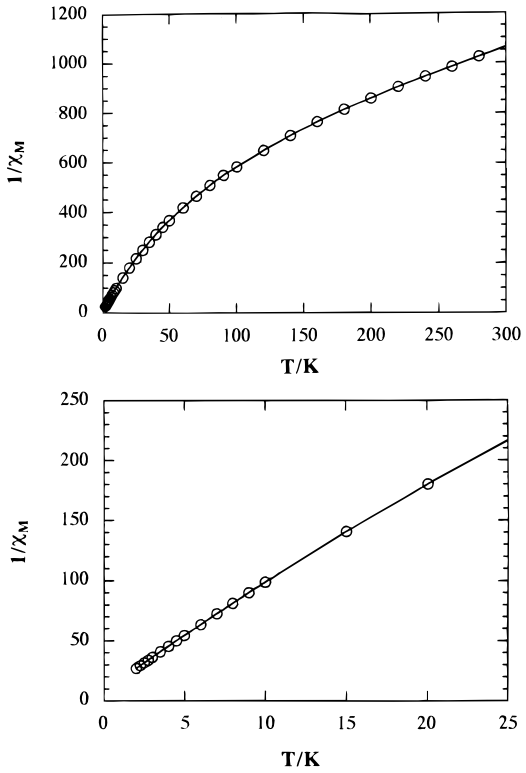

Figure 9. Inverse molar magnetic susceptibility ($1/\chi_M$) plotted against temperature (2−300 K) for $CsCuCeS_3$ (1000 G). (B) Expanded view of the region 2−25 K.

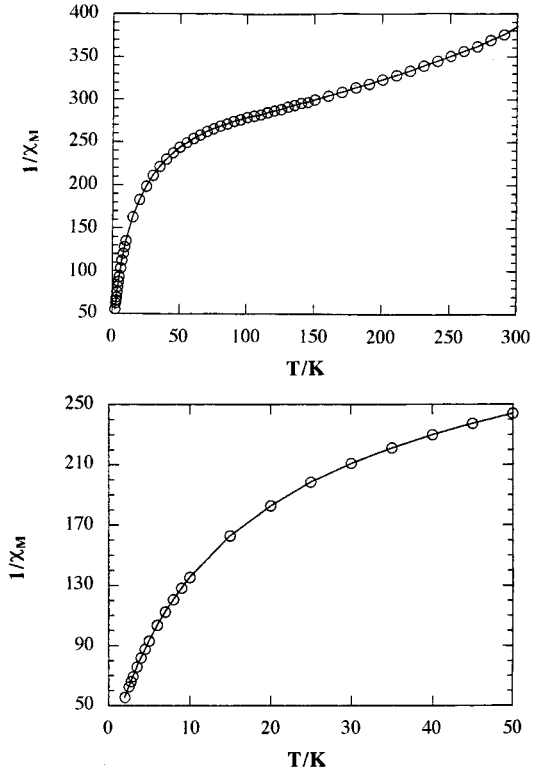

Figure 10. Inverse molar magnetic susceptibility ($1/\chi_M$) plotted against temperature (2−300 K) for $KCuUSe_3$ (5000 G). (B) Expanded view of the region 2−50 K.

known to result in metallic conductivity in several alkali metal/copper/chalcogenides (for example, KCu_4S_3[38]). The apparent presence of holes in the conduction band of $K_2Cu_2CeS_4$ results in appreciable conductivity.[20] Rather, some mechanism was at work to retard carrier mobility in the phase, as evidenced by unusual thermopower measurements.[20] $CsCuCeS_3$, therefore, is also a valence fluctuation compound and presents an opportunity to study, through magnetic and charge-transport experiments, the effects of holes in the conduction band of a second mixed Cu/Ce compound with a different structure type (see below).

Mixed oxidation states on the chalcogenides of $KCuUSe_3$ are not expected. U^{4+} is very common in all its chalcogenide chemistry, and so with the formalism $K(Cu^+)(U^{4+})(Se^{2-})_3$, the compound is expected to be a semiconductor.

Magnetic Susceptibility. The magnetic response of $CsCuCeS_3$ can be used to support the $Cs(Cu^+)(Ce^{3+})(S^{2-})_2(S^-)$ formalism. The temperature-dependent magnetic susceptibility of $CsCuCeS_3$ is shown in Figure 9. Empirically, it is very similar to that of $K_2Cu_2CeS_4$; the plot of $1/\chi_M$ vs T has a continually changing slope but one which increases more rapidly below 150 K than above. Quantitatively, however, the data are quite different. Over several trials, the average μ_{eff} (from 160−300 K) was found to be 1.8 μB, much less than both the theoretically and experimentally expected values. A large θ value is also present (−150 K). Although the presence of paramagnetism rules out the formalism invoking a Ce^{4+}, which would result in a diamagnetic material (i.e., $Cs(Cu^+)(Ce^{4+})(S^{2-})_3$), the exact nature of the oxidation states remains unclear, consistent with valence fluctuations in this compound.

The large negative value for θ indicates a large amount of local antiferromagnetic ordering, and if such an effect is carrying over to the room-temperature regime, then this may also serve to drive down the μ_{eff}. The magnetic response of $K_2Cu_2CeS_4$ also exhibited a large θ (−440 K) but possessed a more conventional μ_{eff} (2.38 μB). Although both structures feature Ce^{3+} cations in octahedra of S atoms, in $K_2Cu_2CeS_4$, these octahedra edge-share in one dimension whereas those in $CsCuCeS_3$ form a two-dimensional network of edge- and corner-sharing octahedra. The extended Ce−S bonding in $CsCuCeS_3$ is enhancing sulfur-mediated antiferromagnetic superexchange between the Ce^{3+} cations, leading to the low μ_{eff} values. As in $K_2Cu_2CeS_4$, a hole in the sulfur 3p band may also be playing a role in facilitating this exchange as is thought to occur in the spinel compounds $CuCr_2Q_4$ (Q = S, Se, Te).[39]

The magnetic behavior of $KCuUSe_3$ is somewhat more straightforward. The $1/\chi_M$ vs T plot of data taken at 5000 G (Figure 10) is actually similar to that of $CsCuCeS_3$ in that the data have no straight-line region but change slope much more dramatically as the temperature is lowered. For T > 150 K, a μ_{eff} of 3.65 μB and a θ of −378 K were estimated by fitting a straight line to the data. The μ_{eff} is consistent with that expected for a U^{4+} (3.58 μB),[32] and the value for θ indicates a large amount of local antiferromagnetic ordering. The rapidly changing slope of the data at low temperature suggests that the U^{4+} is experiencing some of the same crystal-field effects in this lattice that are observed for Ce^{3+} in $K_2Cu_2CeS_4$ and $CsCuCeS_3$. Because the 5f orbitals are less shielded by the valence electrons than the more contracted 4f orbitals of the lanthanides, U^{4+}

(38) Brown, D. B.; Zubieta, J. A.; Vella, P. A.; Wrobleski, J. T.; Watt, T.; Hatfield, W. E.; Day, P. *Inorg. Chem.* **1980**, *19*, 1945−1950.

(39) (a) Lotgering, F. K.; van Stapele, R. P. *J. Appl. Phys.* **1968**, *39*, 417. (b) Hollander, J. C. Th.; Sawatzky, G.; Haas, C. *Solid State Commun.* **1974**, *15*, 747−751.

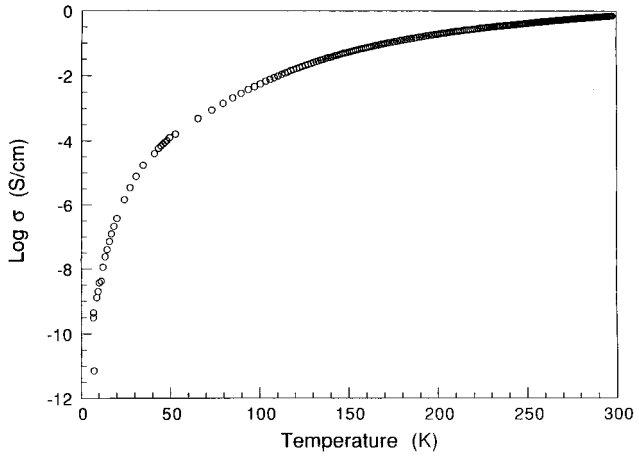

Figure 11. Conductivity log σ (S/cm) plotted against temperature (K) for a pressed pellet sample of $CsCuCeS_3$.

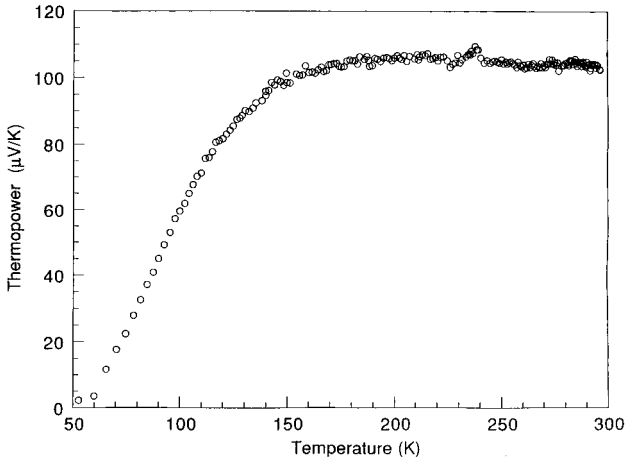

Figure 12. Thermopower (μV/K) plotted against temperature (K) for a pressed pellet sample of $CsCuCeS_3$.

has exhibited pronounced crystal-field effects in several dilute salt paramagnetic compounds such as $UX_4 \cdot 4MeCN$ (X = Cl, Br), $UCl_4 \cdot 2Et_2NH$, and others[40] The influence of a crystal field can also have a dramatic effect on the μ_{eff} of the compound. Many of the salts mentioned above have quite low μ_{eff} values (2.61−2.92 μB[40]), but in various transition metal/U/chalcogenide solid-state compounds, μ_{eff} values for the U^{4+} were estimated from 3.0−3.6 μB.[41]

Spectroscopy. Being black, both $KCuUSe_3$ and $CsCuCeS_3$ showed total absorbance in their diffuse reflectance spectra (500−2500 nm). This indicates bandgaps lower than 0.5 eV.

The far-IR spectrum of $CsCuCeS_3$ shows four strong peaks at 288, 262, 227, and 205 cm^{-1}. All of them can be reasonably assigned as Ce−S vibrations since peaks in this region have been observed in the spectra of other Ce/S compounds. The region in which the stretching vibrations of Cu−S are commonly seen (ca. 430 cm^{-1}) remains blank. For $KCuUSe_3$, three strong peaks at 195, 190, and 145 and one very weak one at 130 cm^{-1} are all in the realm of previously seen U−Se vibrations. For example, in K_4USe_8 peaks were observed at 168 and 153 cm^{-1}.[1a] No other spectral features are present, and so the Cu−Se bands remain unobserved as did the Cu−S bands of $CsCuCeS_3$.

Charge-Transport Measurements. Although crystals of $CsCuCeS_3$ grown by these molten salt methods are of sufficient size for diffraction studies, they are too small for use in charge-transport measurements, and so measurements had to be performed on pressed polycrystalline pellets. In $CsCuCeS_3$ the conductivity was nearly 1000 times greater than that of $K_2Cu_2CeS_4$. Figure 11 shows a plot of conductivity vs temperature for such a sample of $CsCuCeS_3$. The data exhibit an increasing conductivity with increasing temperature, the characteristic property of semiconductors. This may arise because of the polycrystalline nature of the pressed pellet samples in which current must traverse the grain boundaries between crystallites, a thermally activated process. Despite this, a fairly high conductivity is achieved at room temperature: 1 S/cm. In general, polycrystalline pressed pellets are 100−1000 times less conductive than single crystals, and so a conductivity of 1000 S/cm could, in fact, be possible. Although the chains of corner-sharing $[CuS_4]$ tetrahedra are distinctly separated from each other, the slightly greater orbital overlap from the layers of $[CeS_6]$ octahedra in $CsCuCeS_3$, must be just enough to cause a significant change in the compound's band structure, relative to that of $K_2Cu_2CeS_4$, producing high carrier mobility.

The thermopower response of $CsCuCeS_3$ with changing temperature is shown in Figure 12. Thermopower is a zero current technique and thus gives information on the intrinsic charge-transport properties of the sample despite grain boundaries.[42] The positive values for the thermopower indicate holes as the primary charge carriers, consistent with a delocalized S^- oxidation state. Both the magnitude of the thermopower values and the shape of the plot point to something other than a common metallic mechanism at work in the material's conductivity. For a metallic species, the thermopower response is small (<20/μV) and tends toward zero with decreasing temperatures. Whatever that mechanism, there appears to be a transition at 150 K from a temperature-independent thermopower to one which tends toward zero. The magnitude of TP and its T dependence are consistent with a semimetal or a poor metal. Such a property may be the result of very narrow bands near the Fermi level, giving rise to massive carriers. Some type of carrier localization occurs in the form of small polarons, as was discussed for $K_2Cu_2CeS_4$.[20] A more complete understanding of the charge-transport properties of both these phases must wait until crystals of adequate size can be grown for use in a variety of single-crystal measurements.

Unlike $CsCuCeS_3$, large single crystals of $KCuUSe_3$ could be grown from fluxes very rich in Se and at increased reaction temperatures (for example, K_2Se/Cu/U/Se = 1/1/1/24 heated at 450 °C for 2 days). Such crystals were easily manipulated for charge-transport studies. Figure 13 shows conductivity (S/cm) plotted as a function of 1000/T for a typical crystal of $KCuUSe_3$. The increasing conductivity with increasing temperatures shows unambiguously that the compound is semiconducting with a value at 300 K of 0.1 S/cm. From these data the activation energy to charge transport was estimated to be in the range 0.164−0.167 eV. Figure 14 shows the thermopower measurements taken on single crystals of $KCuUSe_3$. The positive values indicate

(40) Siddall, III, T. H. In *Theory and Applications of Molecular Paramagnetism*; Boudreaux, E. A., Mulay, L. M., Eds.; John Wiley and Sons: New York, 1976, p 306.

(41) Noel, H.; Troc, R. *J. Solid State Chem.* **1979**, *27*, 123−135.

(42) Marks, T. J. *Angew. Chem., Int. Ed. Engl.* **1990**, *29*, 857−879.

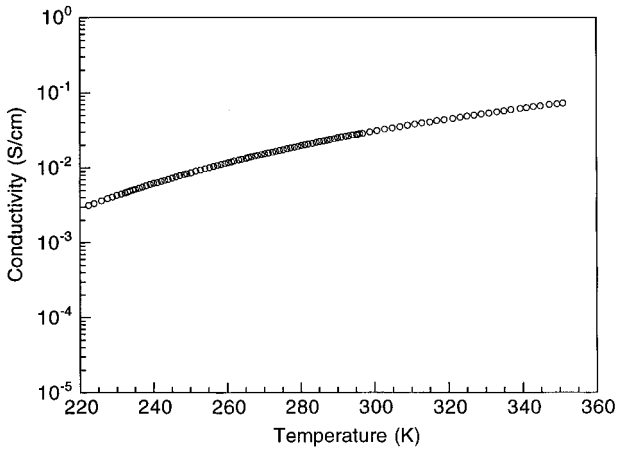

Figure 13. Conductivity log σ (S/cm) plotted against temperature (1000/K) for a single-crystal sample of $KCuUSe_3$.

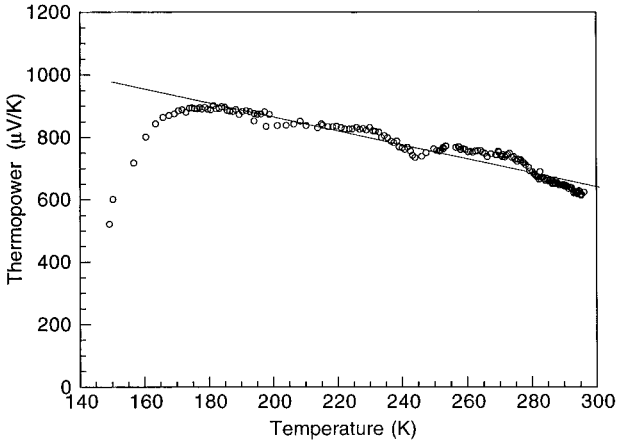

Figure 14. Thermopower (μV/K) plotted against temperature (K) for a single crystal of $KCuUSe_3$.

p-type carriers while the negative slope to the data, and the very high Seebeck coefficient, is characteristic of a semiconductor.

D. Summary and Conclusions

As the Cu/f-block metal ratio in the phases described in this report has increased, there has been a steady and progressive adaptation of the resulting structures to the increased Cu content. In the $ACuM_2Q_6$ phases, which have the smallest Cu/M ratio, the structure is simply an M/Q network, previously observed in $NaLnS_3$,[1c] with Cu^+ "diffused" into tetrahedral sites within the lattice. Aside from pointing to the stability of this particular lanthanide/chalcogenide framework, this result shows how the phase formation was dominated by the lanthanide being in excess of Cu and by the presence of the proper countercation. In compounds where the Cu/M ratio is 1, $ACuMQ_3$, a breakdown of the M-dominated framework is observed. This particular M/Q framework had not been seen previously for the f-block metals under study. At this Cu/M ratio, octahedral coordination about the lanthanides and actinides begins to be observed. In the previously reported phase, $K_2Cu_2CeS_4$, with its Cu/Ce ratio of 2, Cu makes its presence felt by fragmenting the M/Q network from two- to one-dimensional, and the chains of $[CeS_6]$ octahedra are fully separated from one another by intervening $[CuS_4]$ tetrahedra. The chemistry of the f-block element is still very much a factor as $ACuMQ_3$ is the only structure type which has been seen for both a lanthanide and an actinide. However, where the chemistry of the second metal will allow it, the amount of Cu in the reaction produces a pronounced effect on the structural outcome. This suggests that additional new phases may be possible via systematically varying the amount to Cu in the reactions. The present compounds are very selective in that the f-block/Q framework is either fully two- or one-dimensional; no examples were characterized which contained "intermediate" dimensionality (i.e., two one-dimensional chains fusing into a single ribbon). Perhaps such phases could be achieved by running mixed A or mixed M reactions in conjunction with changing amounts of Cu.

Mixed chalcogenide valency was also observed. Not only did this occur when the Cu content was in amounts greater or equal to the f-block metal but also to the alkali metal as well. All phases were also synthesized in very basic fluxes, giving rise to their exclusively monochalcogenide environments. As previously noted in the discussion of these compounds, there exist many examples of A/Cu/Q phases which have been shown to possess mixed Q^{2-}/Q^- oxidation states, and this property of Cu is clearly transferring to this new Cu/f-block chemistry. An apparent requirement is that the f-block element involved have some high oxidation state available which is not stable in chalcogenide environments; although Ce^{3+} forms mixed S^{2-}/S^- phases in both $K_2Cu_2CeS_4$ and $CsCuCeS_3$, simple elemental substitution with La^{3+} did not yield the expected analogues. The holes in the conduction band which result from mixed S^{2-}/S^- states imparts high electronic conductivity to the phases. Although a full investigation is somewhat hampered by the lack of large single crystals suitable for charge-transport studies, there is evidence that these phases possess a conductivity that is not of the classical metallic mechanism but that does appear to be closely tied to structure.

Acknowledgment. This research was made possible with funding from NSF Grants DMR-92-02428 and DMR-95-27347. At NU this work made use of Central Facilities supported by NSF through the Materials Research Center (DMR-91-20521). M.G.K. is an A. P. Sloan Foundation Fellow and a Camille and Henry Dreyfus Teacher Scholar.

Supporting Information Available: Calculated and observed X-ray powder diffraction patterns, and anisotropic thermal parameters (15 pages); listings of calculated and observed structure factors for $CsCuCe_2S_6$, $KCuCe_2Se_6$, $K_2Cu_2CeS_4$, $CsCuCeS_3$, and $KCuUSe_3$ (13 pages). Ordering information is given on any current masthead page.

CM950438B